EPR and NMR Spectra as Probes of Spin-Density Distributions in Heterocyclic Ligands Coordinated in trans-[L(Im)(NH3)4RuIII]: Crystal Structure of trans-[(Im)2(NH3)4Ru]Cl3.cntdot.H2...

ARTICLE *in* JOURNAL OF THE AMERICAN CHEMICAL SOCIETY · MARCH 1995

Impact Factor: 12.11 · DOI: 10.1021/ja00117a022

6 AUTHORS, INCLUDING:

Peter E Doan
Northwestern University
62 PUBLICATIONS **1,787** CITATIONS
SEE PROFILE

Michael J Clarke
Boston College, USA
84 PUBLICATIONS **3,071** CITATIONS
SEE PROFILE

EPR and NMR Spectra as Probes of Spin-Density Distribution in Heterocyclic Ligands Coordinated in *trans*-[L(Im)$(NH_3)_4Ru^{III}$]: Implications for Long-Range Electron Transfer. Crystal Structure of *trans*-[$(Im)_2(NH_3)_4Ru]Cl_3 \cdot H_2O$

K. J. LaChance-Galang,[†] Peter E. Doan,*[,‡] M. J. Clarke,*[,†] U. Rao,[†] A. Yamano,[†] and Brian M. Hoffman[‡]

Contribution from the Merkert Chemistry Center, Boston College, Chestnut Hill, Massachusetts 02167, and Department of Chemistry, Northwestern University, Evanston, Illinois 60208

Received August 2, 1994[⊗]

Abstract: Spectroscopic studies of *trans*-[(L)(Im)$(NH_3)_4Ru^{III}$], where Im = imidazole and L = isonicotinamide (Isn), pyridine (Py), Im, NH_3, Cl^-, and SO_4^{2-}, indicate that π-bonding by the *trans* ligand significantly affects mixing of the d_π–π (imidazole) orbitals. Analysis of the EPR spectra provides a description of the frontier d_π orbitals involved in electron transfer and estimates of Δ and V (the tetragonal and rhombic distortion parameters, respectively), all of which vary with the π-donor abilities of L. As Δ and V are of the same magnitude as the the spin–orbit coupling parameter, λ, there is extensive spin–orbit mixing of the d_{xz} and d_{yz} and (to a lesser extent) the d_{xy} orbitals. Reduction potentials and energies of imidazole → Ru^{III} charge transfer transitions correlate linearly with the π-donor/acceptor ability of L so that a correlation is also evident between these properties and the ligand field splitting of the t_{2g} manifold, which leads to an unsuspected correlation between the difference between the two largest **g** values, Δg_{12}, and $E°$. Electronic perturbations appear to be transmitted to C5 on the imidazole ring, which is the site linked to Ru-modified proteins used as probes of long-range electron transfer. This implies that variations of the ligand in the *trans* position to modify the $E°$ for the $Ru^{III/II}$ couple can also affect the superexchange coupling involved in electron transfer. *trans*-[$(Im)_2(NH_3)_4Ru^{III}]Cl_3 \cdot H_2O$ crystallizes in the monoclinic space group, $P2_1/n$ (No. 14), with cell parameters $a = 18.111(9)$ Å, $b = 7.187(2)$ Å, $c = 14.352(7)$ Å, $\beta = 113.26(4)°$, and $Z = 4$ and exhibits an eclipsed conformation of the imidazole rings. MM2 and IEHT calculations suggest why the eclipsed conformation is slightly favored over the staggered and that the imidazole rings freely rotate in solution.

Introduction

An effective method of probing the distance dependence of long-range electron transfer (ET) in proteins has been to attach ammineruthenium centers to histidyl imidazoles at predetermined distances from the native redox site. This approach also allows the electron transfer rates to be studied as a function of driving force by varying π-acceptor ligands on the ruthenium.[1] The electron transfer rate between the two redox centers is expressed by

$$k_{ET} = \sqrt{\frac{\pi}{h^2 \lambda k_B T}} \mathbf{H}_{AB}^2 e^{-\frac{(\Delta G° + \lambda)^2}{4\lambda k_B T}}$$

where $\Delta \mathbf{G}°$ is the electrochemical driving force, λ is the reorganization energy, and $\mathbf{H}_{AB}$ is the electronic coupling, whose magnitude varies with the separation and medium intervening between the donor/acceptor pair.[2] $\mathbf{H}_{AB}$ also depends on the delocalization of the frontier ruthenium d_π orbital onto the histidylimidazole, which links the metal to the protein. Since histidylimidazoles are bound to the peptide chain through C5, variations in the coefficient of the donor/acceptor MO at this position must affect long-range electron transfer rates.

NMR studies of [$L(NH_3)_5Ru^{III}$] (d^5; $S = 1/2$), where L = imidazole, pyridine, purine, and pyrimidine derivatives, indicate that the paramagnetic shifts of ring protons are strongly dependent on ring substitutions. Consequently, it is reasonable to expect that the ligands used to adjust the reduction potential of the ruthenium center[1] also transmit π-electronic effects into the imidazole ring that would affect coupling through C5.

In this study, the ligand *trans* to the imidazole in *trans*-[L(Im)-$(NH_3)_4Ru^{III}$] has been systematically varied so as to modulate $E°$. These changes are correlated with parallel changes in the charge transfer transitions, EPR spectra, and ligand field splittings derived from these spectra and ^1H NMR spectra. In addition, the unexpected finding of an eclipsed conformation for the π-donor and π-acceptor heterocyclic ligands in *trans*-[(Isn)(Im)$(NH_3)_4Ru](CF_3CO_2)_3$[2] prompted an examination of the arrangement between the two π-donor ligands in *trans*-[$(Im)_2$-$(NH_3)_4Ru]Cl_3$ and a consideration of the relative energies of the eclipsed and staggered conformations.

Experimental Section

Syntheses. $RuCl_3$ was purchased from Johnson Matthey. Imidazole (Im), isonicotinamide (Isn), and pyridine (Py) were purchased from Aldrich and used without further purification. The compounds *trans*-[$Cl(SO_2)(NH_3)_4Ru]Cl$,[3] *trans*-[$(SO_4)(Py)(NH_3)_4Ru]Cl$, *trans*-[(SO_4)(Isn)-$(NH_3)_4Ru]Cl$, and *trans*-[$(SO_4)(Im)(NH_3)_4Ru]Cl$ were prepared by literature methods.[4]

***trans*-[(Isn)(Im)$(NH_3)_4Ru]Cl_3$** was synthesized by dissolving *trans*-[(SO_4)(Isn)$(NH_3)_4Ru]Cl$ in a minimum of water and reducing it with zinc amalgam for 20 min under an argon atmosphere. A 2:1 molar ratio of imidazole was added to the solution, and reduction was continued for 3 h to give a dark reddish-brown solution. The zinc amalgam and undissolved ligand were filtered off, and a 50/50 mixture

[†] Boston College.
[‡] Northwestern University.
[⊗] Abstract published in *Advance ACS Abstracts,* February 15, 1995.

(1) Winkler, J. R.; Gray, H. B. *Chem. Rev.* **1992**, *92*, 369.
(2) Wishart, J. F.; Zhang, X. a.; Isied, S. S.; Potenza, J. A.; Schugar, H. J. *Inorg. Chem.* **1992**, *31*, 3179–3181.
(3) Vogt, L. H.; Katz, J. L.; Wiberly, S. E. *Inorg. Chem.* **1965**, *4*, 1157.
(4) Isied, S. S.; Taube, H. *Inorg. Chem.* **1976**, *15*, 3070–3075.

0002-7863/95/1517-3529$09.00/0

of 30% H_2O_2/3 M HCl was added dropwise until the solution turned from deep red to reddish-orange. Acetone was added to induce precipitation, and the solution was cooled for several hours. The product was then filtered, redissolved, and chromatographed on SP-Sephadex. The band of interest eluted with 3 M HCl. The volume was reduced by rotary evaporation, and acetone was added to precipitate the product as an orange powder. Needle-like crystals were obtained by acetone diffusion. Anal. Calcd for *trans*-[Im$(SO_4)(NH_3)_4$Ru]Cl·3.5H_2O: C, 20.44; H, 5.54; N, 21.19; Cl, 20.11. Found: C, 20.70; H, 5.41; N, 20.91; Cl, 20.10. UV−vis (λ_{max}, nm (ϵ, M^{-1} cm^{-1})): 265 (6380), 305 sh (4790), 475 (251).

***trans*-[(Py)(Im)$(NH_3)_4$Ru]Cl_3** was similarly prepared from *trans*-[Py$(SO_4)(NH_3)_4$Ru]Cl. Anal. Calcd for [(Py)(Im)$(NH_3)_4$Ru]Cl_3H_2O: C, 21.80; H, 5.27; N, 22.25; Cl, 24.13. Found: C, 21.98; H, 5.24; N, 21.98; Cl, 23.84. UV−vis (λ_{max}, nm (ϵ, M^{-1} cm^{-1})): 248 (6690), 310 (3440), 456 (277).

***trans*-[$(Im)_2(NH_3)_4$Ru]Cl_3** was similarly prepared from *trans*-[(SO_4)(Im)$(NH_3)_4$Ru]Cl. Orange needle-like crystals were obtained by acetone diffusion. Anal. Calcd for [$(Im)_2(NH_3)_4$Ru]Cl_3·H_2O: C, 16.77; H, 5.17; N, 26.08; Cl, 24.75. Found: C, 17.10; H, 5.14; N, 26.18; Cl, 24.77. UV−vis (λ_{max}, nm (ϵ, M^{-1} cm^{-1})): 311 (5350), 435 (661).

***trans*-[(Cl)(Im)$(NH_3)_4$Ru]Cl_2** was prepared by zinc amalgam reduction of a solution of *trans*-[(SO_4)(Im)$(NH_3)_4$Ru]Cl in 2 M HCl under argon for 1 h. The zinc was then removed, and a 50/50 mixture of 30% H_2O_2/3 M HCl was added dropwise until the solution turned yellow. Acetone was then added to induce precipitation. The product was filtered, redissolved, and chromatographed on SP-Sephadex. The band of interest eluted with 0.3 M HCl. A pale yellow powder was obtained upon rotary evaporation. Needle-like crystals formed upon acetone diffusion. Anal. Calcd for [(Cl)(Im)$(NH_3)_4$Ru]Cl_2·H_2O: C, 9.96; H, 5.03; N, 23.24; Cl, 29.90. Found: C, 9.89; H, 4.79; N, 23.01; Cl, 29.84. UV−vis (λ_{max}, nm (ϵ, M^{-1} cm^{-1})): 330 (3110), 400 sh (280).

Physical Measurements. Elemental analyses were done by Robertson Laboratories Inc. ^1H NMR spectra were obtained in 5 mm NMR tubes on a Varian Unity 300 MHz FT spectrometer. Protons were removed by dissolving samples (~10 mg) in D_2O, followed by lyophilization (three times) before dissolution in 0.5−0.7 mL of D_2O. pK_a determinations were performed by adjusting the pH (uncorrected) with dilute solutions of NaOD and DCl.

Dispersion-mode EPR spectra were collected under rapid-passage conditions at 2 K with both X-band (9.5 GHz) and Q-band (35 GHz) spectrometers. 77 K EPR spectra were obtained on a highly modified Varian E-4 spectrometer. The Q-band EPR/ENDOR instrument has been described previously.[10] The X-band spectra were obtained using a Bruker ER-200 spectrometer and a cavity described previously.[5] The complexes were dissolved in a 30−70% (v/v) ethylene glycol−water mixture with the pH adjusted to pH = 5−6. The final concentrations were approximately 1 mg mL^{-1}. A background copper EPR signal that originated in the cavity was digitally subtracted from all X-band spectra. Because the magnets have a limit of 1.5 T, only **g** values greater than 1.7 could be obtained at the Q-band. All compounds studied show EPR spectra at 77 K with reasonable signal to noise ratios in both neat solid samples and dilute frozen solutions; however, the lines are rather broad. The advantages of using adiabatic rapid-passage conditions for such broad EPR signals have been discussed.[6]

UV-vis spectra were run on a Cary 2400 spectrophotometer. Spectrophotometric pK_a determinations were done by spectrophotometric titrations at an ionic strength of 0.1 M LiCl.

Electrochemistry was performed on 1−3 mM solutions in 0.1 M LiCl on a potentiostat interfaced to an IBM-PS2 running ASYST programs created in this laboratory. Reduction potentials were first examined by cyclic voltammetry to ascertain the reversibility of each couple and then measured by square wave voltammetry from peak positions relative to an internal standard, [$(NH_3)_6Ru^{III/II}$] (57 mV). The working electrode was carbon paste, the reference electrode was Ag/AgCl, and the counter electrode was platinum wire.

Table 1. Crystallographic Data for *trans*-[$(Im)_2(NH_3)_4$Ru]Cl_3·H_2O

formula	$H_{22}C_6N_8OCl_3Ru$
formula weight	429.72
T (°C)	23(1)
space group, crystal system	$P2_1/n$ (No. 14), monoclinic
cell constants	
a (Å)	18.111(9)
b (Å)	7.187(2)
c (Å)	14.352(7)
β (deg)	113.26(4)
cell volume (Å^3)	1716(1)
Z (fw/unit cell)	4
crystal dimensions (mm)	0.20 × 0.20 × 0.30
radiation source (graphite monochromated)	Mo $K\alpha$ (λ = 0.710 69 Å)
d_{calcd} (g/cm^3)	1.663
μ (cm^{-1}), rel trans. factors	13.73, 0.94−1.0
$R = \sum(\|F_o\| - \|F_c\|)/\sum\|F_o\|$	0.040
$R_w{}^b = [\sum w(\|F_o\| - \|F_c\|)^2/\sum w\|F_o\|^2]^{1/2}$	0.045
goodness of fit = $\sum w(\|F_o\| - \|F_c\|)/\sigma/(N_{obs} - N_{parameters})$	1.09

[a] Reflections with $I_o > 3\sigma(I_o)$ were retained as observed and used in the solution and refinement of the structure. Three standard reflections were monitored with a limit of 0.2% variation. Function minimized $\sum w(|F_o| - |F_c|)^2$. [b] Weighting scheme: $w = 4(F_o)^2/[\sigma^2(F_o)^2]$. [c] All calculations were performed by using the TEXSAN-TEXRAY Structure Analysis Package, Molecular Structure Corp., 1985. No decay correction was necessary. Hydrogen atoms were found in difference maps and included in idealized positions (N−H = 0.87 Å), with thermal parameters 20% greater than the B_{equiv} value of the atoms to which they were bonded. Refinement was by full-matrix least-squares.

Crystal Structure. Pertinent crystal data for *trans*-[$(Im)_2(NH_3)_4$-Ru]Cl_3·H_2O are given in Table 1 with crystal coordinates listed in supplementary Table S-I. Single crystals of *trans*-[$(Im)_2(NH_3)_4$Ru]-Cl_3·H_2O were grown by slow vapor diffusion of acetone into an aqueous solution of the compound. A suitable crystal mounted on a glass fiber was placed in the beam of a Rigaku AFC5R diffractometer. Space group assignment was based on the systematic absences of $h0l$, $h + l \neq 2n$, and $0k0$, $k \neq 2n$. The Ru atom was located by the Patterson method. Other atoms (including all hydrogens) were located from difference Fourier maps.[39,40] The non-hydrogen atoms were refined anisotropically and hydrogen atoms isotropically by full-matrix least-squares. An empirical absorption correction (ψ-scan) was applied. Neutral atom scattering factors and anomalous dispersion effects were included in F_{calc};[38] the values for $\Delta f'$ and $\Delta f''$ were those of Cromer.[7]

MO and MM Energy Calculations. ZINDO (INDO/1),[8] IEHT,[9] and MM2[10] were performed on a CaChe workstation[11] by using the crystallographic coordinates in Table S-I or idealized structures with Ru−N bond distances of 2.101 Å for ammonia, 2.048 Å for imidazole, and 2.089 Å for pyridine. Odd-electron IEHT calculations were run as singlets using a restricted Hartree−Fock function.

EPR Parameters. The analysis of the **g** values seen in low-spin d^5 systems is done hierarchically. The six ligands set up a ligand field whose main component is of cubic symmetry and splits the five d orbitals into a high-lying e_g doublet and a lower t_{2g} triplet. Lower-symmetry ligand field components that split the t_{2g} triplet, defined by the ligand field perturbation Hamiltonian, **V**, and the spin−orbit coupling, λ**LS**, are of the same magnitude and must be treated on an equal footing. Of the numerous similar mathematical approaches that have been published,[12−17] we have chosen to combine the concise

(5) Cline, J.; Reinhammar, B.; Jensen, P.; Venters, R. A.; Hoffman, B. M. *J. Biol. Chem.* **1983**, *258*, 5124.
(6) Mailer, C.; Taylor, C. P. S. *Biochim. Biophys. Acta* **1973**, *322*, 195−203.
(7) Cromer, D. T.; Weber, J. T. *International Tables for X-ray Crystallography*; Kynoch Press: Birmingham, AL, 1974; Vol. IV, Tables 2.2 A and 2.3.1.
(8) Anderson, W. P.; Cundarai, T. R.; Drago, R. S.; Zerner, M. C. *Inorg. Chem.* **1990**, *29*, 1−3.
(9) Hoffmann, R. *J. Chem. Phys.* **1963**, *39*, 1397−1412.
(10) Allinger, N. L. *J. Am. Chem. Soc.* **1977**, *99*, 8127.
(11) *CAChe, ZINDO*, Version 2.8; Terra Pacific Writing Corp.: Beaverton, OR 97075, 1991.
(12) Bleaney, B.; O'Brien, M. C. M. *Proc. Phys. Soc., London, Sect. B* **1956**, *69*, 1216−1230.
(13) Bohan, T. L. *J. Magn. Reson.* **1977**, *26*, 109−118.
(14) Griffith, J. S. *Mol. Phys.* **1971**, *21*, 135−139.
(15) Kotani, M. In *The Structures and Properties of Biomolecules and Biological Systems*; Interscience: London, 1964; pp 159−181.
(16) Taylor, C. P. S. *Biochim. Biophys. Acta* **1977**, *491*, 137−149.

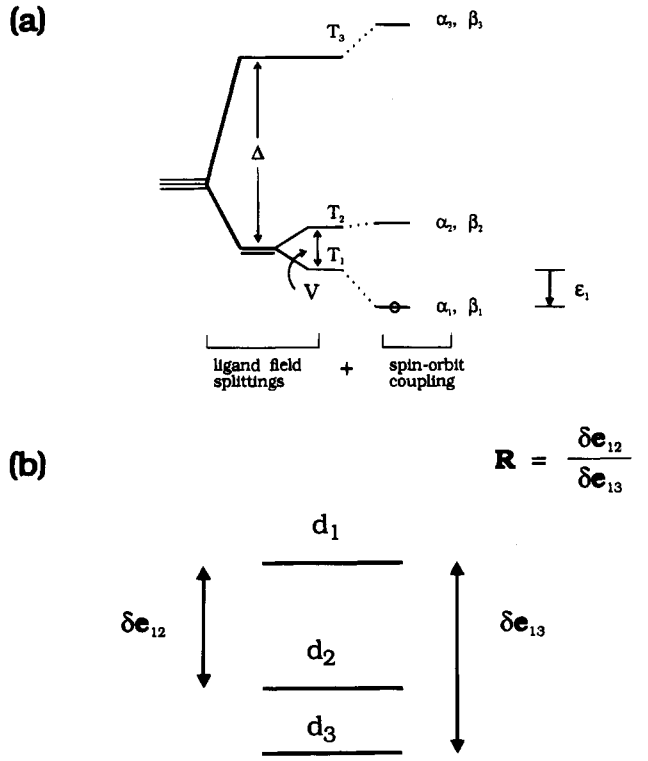

Figure 1. (a) Energy level splitting diagram for a t_{2g}^5 system in the hole formalism. The standard parameterization of the ligand field splittings (Δ, V) is shown for a tetragonally elongated case ($\Delta < 0$ for holes configuration or $\Delta > 0$ for electrons). The electronic configurations of the ligand field only Hamiltonian are denoted by (T_1, T_2, T_3) rather than by symmetry labels (see text). The eigenstates of the ligand field + spin−orbit coupling Hamiltonian are denoted by the Kramer's doublets ($|\alpha>_j$, $|\beta>_j$) where $j = 1$, 2, and 3 and $\epsilon_1 < \epsilon_2 < \epsilon_3$. Values of ϵ_j are given relative to T_1. (b) Diagram using the electron formalism indicating the definition of R (fraction of tetragonal elongation) is defined in terms of the ligand field only energy levels: $R = \delta e_{12}/\delta e_{13}$ or $R = 2|V|/(|V| + 2|\Delta|)$ when $\Delta < 0$, and $R = (2|\Delta| - |V|)/(2|\Delta| + |V|)$ when $\Delta > 0$.

method of Taylor,[13] where the ligand field eigenstates of **V** are the cubic t_{2g} orbitals (d_{xy}, d_{xz}, d_{yz}) and x, y, and z lie along the the ligand−atom axes, with that of Bleaney and O'Brien,[12] which allows the eigenstates of **V** to consist of linear combinations of the cubic orbitals. The important difference between the present formalism and that of Taylor is that the axis system employed here is rotated by 45° about the z-axis (vide infra) so that the d_{xy} orbital becomes the $d_{x^2-y^2}$.

The standard parameterization of the ligand field energies involves two energy parameters expressed as multiples of the spin−orbit interaction. These are (1) a tetragonal distortion parameter, Δ, and (2) a rhombic distortion parameter, V, (see Figure 1). A proper axis system can always be defined such that $|^2/_3\Delta| \geq |V|$ and Δ is taken to define the **g** tensor z-axis.[18] However, the wide range of magnetic anisotropies observed in this study makes this parameterization confusing. Instead, it is simpler to use a pair of parameters that are defined in terms of the three eigenvalues of the ligand field perturbation Hamiltonian, **V**, so as to be positive and contain no implicit assumptions about axis orientations. These three eigenstates of **V**, which need not be specified here, are labeled simply d_1, d_2, and d_3 in the electron formalism and T_1, T_2, and T_3 in the hole formalism (Figure 1a), which was used in the calculations. For reasons discussed below, the set (d_1, d_2, d_3) is taken to correspond to a permutation of the orbitals (d_{xz}, d_{yz}, $d_{x^2-y^2}$). Eigenvalues are ordered $e_1 \geq e_2 \geq e_3$ in the electron formalism (Figure 1b), and the discussion is presented in these terms.

The two ligand field splitting energies are defined as differences from the eigenvalues of the HOMO (d): δe_{12} and δe_{13} (Figure 1b).

(17) Weissbluth, M. In *Hemoglobin*; Springer-Verlag: New York, 1974; pp 99−105.

(18) Blumberg, W. E. In *Magnetic Resonance in Biological Systems*; Ehrenberg, A., Malmstrom, B. G., Vanngard, T., Eds.; Pergamon: New York, 1967; p 119.

Table 2. Selected Bond Distances (Å) for *trans*-$[(Im)_2(NH_3)_4Ru]Cl_3 \cdot H_2O$

atom	atom	distance	atom	atom	distance
Ru	N1	2.046(4)	N2	C4	1.373(6)
Ru	N2	2.051(4)	N2	C6	1.317(7)
Ru	N5	2.101(5)	N3	C1	1.327(6)
Ru	N6	2.085(5)	N3	C2	1.357(8)
Ru	N7	2.108(5)	N4	C5	1.342(8)
Ru	N8	2.113(5)	N4	C6	1.343(7)
N1	C1	1.325(6)	C2	C3	1.346(8)
N1	C3	1.379(6)	C4	C5	1.346(8)

Table 3. Reduction Potentials for $[(L)(L')(NH_3)_4Ru^{III}]$ vs NHE

	E (V)	
complex L−L′	imidazole	imidazolate
trans-Im−SO_4^{2-}	−0.025	−0.197
trans-Im−Cl^-	0.025	−0.178
trans-Im−Im	0.121	−0.202
trans-Im−NH_3	0.110	−0.080
trans-Im−Py	0.258	0.154
trans-Im−Isn	0.330	0.232
trans-NH_3−Py[a]	0.300	

[a] Taken from ref 41.

These splittings are used to define two ligand field parameters, δe_{13} and R ($R = \delta e_{12}/\delta e_{13}$) so that $0 \leq R \leq 1$. These quantities are related to the parameter set (Δ, V) through the relationships given in Table 5. The relation between R and the **g** values is illustrated in Figure 2. By convention, when $\delta e_{12} < \delta e_{23}$ ($R < 0.5$), the system is termed tetragonally compressed (which corresponds to $\Delta < 0$ in the standard treatment) and when $\delta e_{12} > \delta e_{23}$ ($R > 0.5$), the system is tetragonally elongated (corresponding to $\Delta > 0$). This is so that R can be seen as a measure of the fraction of tetragonal elongation, with $R = 0$ being a system that is perfectly tetragonally compressed and $R = 1$ defining a perfectly tetragonally elongated system.

The three electronic configurations, $(d_{xz})^1(d_{yz})^2(d_{x^2-y^2})^2$, $(d_{xz})^2(d_{yz})^1(d_{x^2-y^2})^2$, and $(d_{xz})^2(d_{yz})^2(d_{x^2-y^2})^1$, are denoted in the hole formalism by the odd-electron hole states, T_{xz}, T_{yz}, and $T_{x^2-y^2}$, respectively.[19] The product of the three odd-electron hole states (T_{xz}, T_{yz}, $T_{x^2-y^2}$) with the two electron spin wave functions ($m_s = +^1/_2$, $m_s = -^1/_2$) create a basis set of six wave functions. The eigenstates of the complete zero-field Hamiltonian $(-\mathbf{V} - \lambda\mathbf{LS})^2$ are three pairs of degenerate hole states with energies $\epsilon_1 < \epsilon_2 < \epsilon_3$, with wave functions given by

$$|\alpha>_j = -a_j|T_{xz}, +^1/_2> + (ib_j)|T_{yz}, +^1/_2> + c_j|T_{x^2-y^2}, -^1/_2>$$

$$|\beta>_j = a_j|T_{xz}, -^1/_2> + (ib_j)|T_{yz}, -^1/_2> + c_j|T_{x^2-y^2}, +^1/_2>$$

where $j = 1$, 2, and 3 and the coefficients (a_j, b_j, c_j) can be taken to be real.

Application of a magnetic field removes the degeneracy between the ($<\alpha|$, $<\beta|$) pairs and gives rise to the energy splittings observed in the EPR. The **g** values for a configuration in which one of these Kramers doublets are calculated from the standard Zeeman Hamiltonian, $H_z = \beta_e(2\mathbf{S} + k\mathbf{L})\mathbf{B}$, where $k = 1$, are

$$g_{xj} = 2[(b_j + c_j)^2 - a_j^2]$$

$$g_{yj} = 2[b_j^2 - (a_j + c_j)^2]$$

$$g_{zj} = 2[(a_j + b_j)^2 - c_j^2]$$

For the ground state, only the $j = 1$ coefficients apply. Thus, the **g**

(19) Lahiri, G. K.; Bhattacharya, S.; Ghosh, B. K.; Chakravorty, A. *Inorg. Chem.* **1987**, *26*, 4324−4331.

Table 4. Measured and Calculated **g** Values for $[(L)(L')(NH_3)_4Ru^{III}]$ with Coordination Axes Assigned[a]

L−L′	g_1 (g_1 calcd)	axes	g_2 (g_2 calcd)	axes	g_3 (g_3 calcd)	axes
trans-Im−SO_4^{2-}	2.68 (2.69)	*z*,*y*	2.68 (−2.69)	*z*,*y*	1.21 (−1.21)	*x*
trans-Im−Cl^-	2.86 (2.88)	*z*	2.47 (−2.49)	*y*	(−1.20)	*x*
trans-Im−Im	3.04 (3.05)	*z*	2.20 (−2.18)	*y*	(0.15)	*x*
trans-Im−NH_3	2.98 (2.98)	*z*	2.02 (−2.01)	*y*	(0.63)	*x*
trans-Im−Py	3.26 (3.26)	*z*	1.41 (−1.37)	*y*?	(0.96)	*x*?
trans-Im−Isn	3.28 (3.31)	*z*	1.22 (−1.23)	*y*?	(1.03)	*x*?
trans-NH_3−Py	2.82 (−2.83)		1.86 (1.87)		(0.99)	
trans-Cl−NH_3[c]	2.98 (−3.08)	*z*	1.51 (−1.58)		0.99 (1.05)	
trans-Cl−Cl[d]	3.33		1.54		1.18	
trans-Im^-−Im^-[e]	2.54 (−2.57)		2.46 (2.46)		1.54 (−1.57)	

[a] The observed **g** values are listed as positive quantities, while the calculated **g** values are given the proper sign for the convention used. Where no measured **g** value is given, the quantity was not observed experimentally. [b] Axis system shown in Figure 4. [c] Taken from ref 36. [d] Taken from ref 42. [e] Fully deprotonated complex. Calculated values were obtained by using $k = 0.89$.

Table 5. Estimated Crystal Field Splitting Energies and State Energies in Units of λ for $[(L)(L')(NH_3)_4Ru^{III}]$[a]

complex	Δ[b]	$\lvert V\rvert$[b,c]	$\lvert V/\Delta\rvert$[b]	$\delta e_{1,3}$[b]	R[b,d]	ϵ_1[e]	ϵ_2	ϵ_3
trans-Im−SO_4^{2-}	2.04	0	0	2.04	1.00	−0.28	1.82	2.54
trans-Im−Cl^-	2.1	0.75	0.36	2.48	0.70	−0.27	1.77	2.81
trans-Im−Im	0.97	0.63	0.65	1.29	0.51	−0.52	0.88	1.60
	(1.44)	(0.68)	(0.47)[a]					
trans-Im−NH_3	−0.79	0.43	0.54	1.01	0.43	−0.62	0.73	1.33
trans-Im−Py	−1.13	0.12	0.11	1.19	0.10	−0.70	0.57	1.46
trans-Im−Isn	−1.22	0.05	0.04	1.26	0.04	−0.72	0.53	1.51
trans-NH_3−Py	−0.6	0.24	0.40[c]	0.72	0.33	−0.73	0.62	1.07
trans-Cl−NH_3	−0.87	0.18	0.21	0.96	0.19	−0.72	0.59	1.26
trans-Im^-−Im^-[f]	2.8	0.4	0.14	3.00	0.87			

[a] Values from IEHT calculations are in parentheses. [b] Value for electron (rather than hole) formalism. [c] The sign of V has been arbitrarily taken as positive. [d] $R = \delta e_{12}/\delta e_{13}$ or $R = 2|V|/(|V| + 2|\Delta|)$ when $\Delta < 0$, and $R = (2|\Delta| - |V|)/(2|\Delta| + |V|)$ when $\Delta > 0$. [e] Values of ϵ_j are given relative to T_1, the lowest-lying ligand field configuration (see Figure 1) in the hole model. [f] Deprotonated complex.

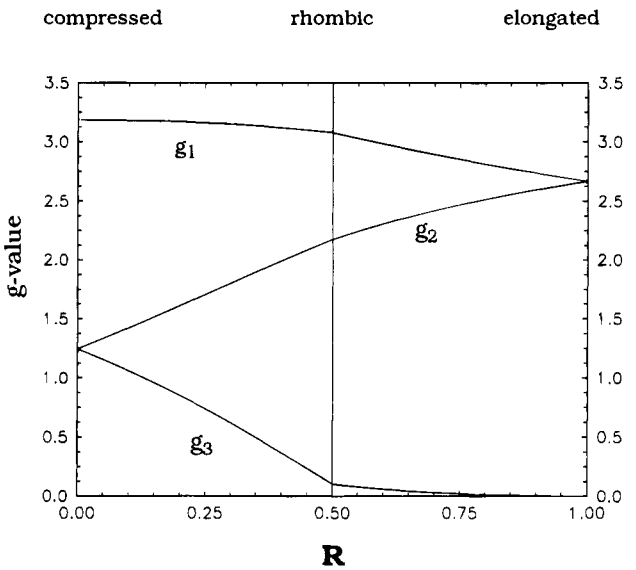

Figure 2. Variation in the absolute values of **g** as a function of R at constant δe_{13}. The **g** values are simply ranked by magnitude ($g_1 > g_2 > g_3$) rather than by symmetry labels (x, y, z). Tetragonally compressed complexes are those with $R \sim 0$, rhombic complexes have $R \sim 0.5$, and tetragonally elongated complexes have $R \sim 1$. In the standard (Δ, V) treatment, the magnetic axis symmetry labels would have $g_1 = g_{x'z'}$ when $R < 0.5$ and $g_3 = g_{x'z'}$ for $R > 0.5$.

values depend on the relative magnitudes of the ligand field splittings and the spin−orbit coupling parameter, λ.

Figure 2 represents a calculation of the ground state **g** values as a function of R for a low-spin d^5 ion where $\delta e_{13}/\lambda = 1$, an appropriate value for this work. The **g** values are designated in the order $g_1 > g_2 > g_3$, rather than by proper symmetry designation ("x, y, z"). For $R = 0$, the center will show an axial **g** tensor with $g_{\parallel} = g_1 = 3.18 > g_{\perp} = g_{23} = 1.25$. As R increases, the g_1 value decreases slowly and

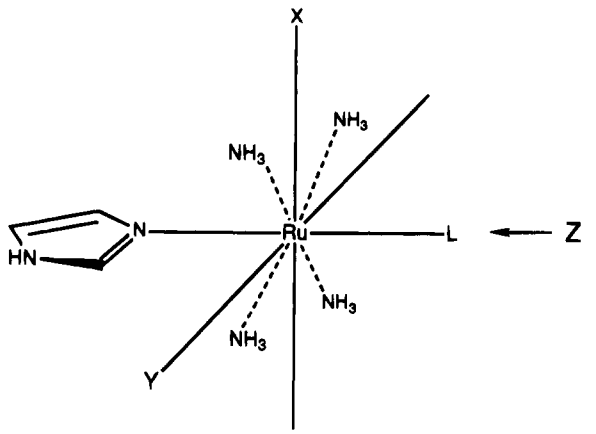

Figure 3. Axis system showing orientation of imidazole ring staggered between ammines.

monotonically until it reaches 3.05 at $R = 0.5$. At small R, a fairly rapid increase in the g_2 value is mirrored by an equally rapid decrease in g_3. At $R = 0.5$, where the ligand field energy levels are equally spaced (complete rhombicity), the g_3 value drops to 0.15 and g_2 increases to 2.20 so that the average of g_2 and g_3 (1.25) has varied only slightly from the $g_{\perp}$ value seen at $R = 0$.

At the other extreme ($R = 1$), the pattern is also axial with $g_{\perp} = g_1, g_2 = 2.70 > g_{\parallel} = g_3 = 0$. As R decreases from 1.0, g_1 and g_2 split almost symmetrically about $g_{\perp} = 2.70$, while g_3 is essentially 0 for $R > 0.5$. The difference between g_1 and g_2 (Δg_{12}) changes almost linearly with R at constant δe_{13}. For $R > 0.2$, where $g_3 < 0.9$, only g_1 and g_2 could be observed in our experiments.

A simple set of rules can be proven to govern the relationships between the ligand field eigenstates, the angular momentum operators, and the order and directions of the **g** tensor in the ground electronic state. The largest **g** value, g_1, lies along the axis that is defined by the non-zero angular momentum operator that connects d_1 and d_2. The second largest **g** value, g_2, lies along the axis defined by the non-zero matrix element between d_1 and d_3. The smallest **g** value direction is defined by the non-zero matrix element between d_2 and d_3. So that if $d_1 = d_{xz}$, $d_2 = d_{yz}$, and $d_3 = d_{x^2-y^2}$, then the directions of the **g** values will be g_1 along z, g_2 along y, and g_3 along x.

Results

Structure. The structure of *trans*-$[(Im)_2(NH_3)_4Ru^{III}]^{3+}$ is shown in Figure 4, and selected bond distances are given in Table 2. In *trans*-$[(Im)_2(NH_3)_4Ru^{III}]Cl_3 \cdot H_2O$, both imidazole rings are planar, with mean deviations of 0.0056 and 0.0014 Å, respectively, for the rings containing N1 and N2. The angle between either imidazole and the plane defined by N1, N2, N5, and N7 is 39(1)°, and the angle between the two imidazole planes is 3.55°. The water molecule in the structure is hydrogen-bonded between ammine protons on N5 and N6 (O−N5, 2.998(7) Å and O−N6, 2.933(7) Å) and Cl2 and Cl3 (O−Cl2, 3.127(5) Å and O−Cl3, 3.106(5) Å). This causes an asymmetry in the packing of the ruthenium complex such that the two

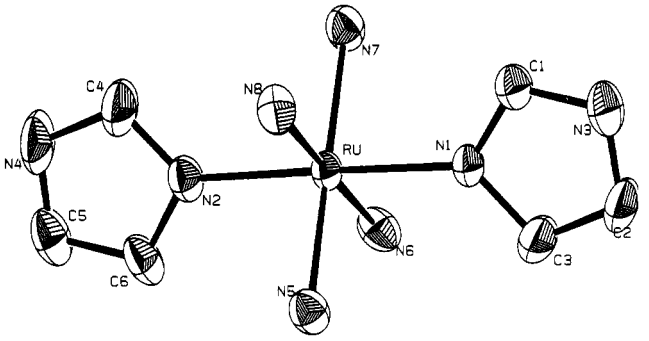

Figure 4. ORTEP diagram of *trans*-$[(Im)_2(NH_3)_4Ru]^{3+}$ showing imidazoles eclipsed with respect to one another but staggered between the ammines.

uncoordinated imidazole nitrogens (N3 and N4) reside on the same side of the structure. There is no significant stacking of the imidazole rings.

UV−Vis Spectra and Electrochemistry. Both IEHT and INDO/1 calculations for *trans*-$[(Im)_2(NH_3)_4Ru^{III}]^{3+}$ indicate rehybridization of the d_{xz} and d_{yz} orbitals such that each is rotated by 45° around the z-axis, resulting in a d'_{xz}, which is perpendicular to the plane of the imidazoles, and a d'_{yz}, which is in the imidazole plane. Henceforth, primes will be dropped and the designations d_{xz} and d_{yz} will refer to the rehybridized d_π orbitals, which are staggered with respect to the Ru−NH_3 bonds. In this new axis system (Figure 3), x and y are oriented between the ammine ligands so that the d_{xy} orbital must be relabeled $d_{x^2-y^2}$. For *trans*-$[(Im)_2(NH_3)_4Ru^{III}]^{3+}$, both IEHT and INDO/1 calculations indicate the HOMO to be predominately d_{xz} in character and to have π-symmetry relative to the imidazole rings. IEHT calculations indicate that d_{yz} and $d_{x^2-y^2}$ are, respectively, 13.1 and 21.2 kJ/mol below d_{xz} in energy, while INDO/1 places d_{yz} and $d_{x^2-y^2}$ substantially below d_{xz} in energy but with about the same energy separation (9.5 kJ) between d_{yz} and $d_{x^2-y^2}$.

The neutral ligand complexes exhibit a broad ligand-to-metal charge transfer (LMCT) absorption band in the 390−475 nm range and a second around 310 nm. By analogy with single-crystal polarized spectra and *ab initio* calculations on complexes of the type $[L(NH_3)_5Ru^{III}]$, where L is an imidazole derivative, these transitions can be assigned as $\pi_1 \rightarrow d_{xz}$ for the visible band and $\pi_2 \rightarrow d_{xz}$ for the near UV transition.[20] The intense absorption in the ultraviolet belongs to a $\pi \rightarrow \pi^*$ ligand absorption. Both the chloro and sulfato complexes exhibit an intense LMCT absorption around 300 nm that arises from the acido ligand and dominates their spectra. The spectra of the *cis* and *trans* bisimidazole complexes differ in that the *cis* complex exhibits an additional LMCT transition (Figure S-1). The pK_a's for imidazole ionization (deprotonation) in *trans*-$[(Im)_2(NH_3)_4Ru^{III}]^{3+}$ are 8.71 and 9.92 as measured spectrophotometrically and verified by monitoring the ^1H NMR shifts as a function of pH.

All complexes exhibited reversible couples as determined by cyclic voltammetry. Reduction potentials are reported relative to NHE in Table 3. As expected, $E°$ values vary directly with the Lever electrochemical parameter (E_L)[21] for the *trans* ligand. Complexes with pyridine ligands were observed to disproportion under basic conditions.

Figure 5 shows an excellent correlation between the energy (E_{LMCT}) of the imidazole $\pi_1 \rightarrow d_{xz}$ transition and the reduction potential of the complex as well as a similar correlation between E_{LMCT} and the Lever parameter (E_L)[21] for the ligand L in $[L(Im)(NH_3)_4Ru^{III}]^{3+}$.

EPR Spectra and Ligand Field Parameters. Figure 6 shows X-band (9.5 GHz) and Q-band (35.1 GHz) dispersion mode, rapid passage EPR spectra of three representative compounds plotted vs **g** value ($\mathbf{g} = h\nu/\beta_e\mathbf{B}$, where $h\nu$ is the microwave quantum and **B** is the magnetic field strength), demonstrating the wide range of magnetic anisotropies observed in this set of compounds. The Q-band spectrum of *trans*-$[Py(Im)(NH_3)_4Ru^{III}]^{3+}$ shows a small amount of an unidentified impurity (ca. 5% in the **g** = 2.0 to 2.3 region), which is not seen in the X-band spectrum. None of the spectra show resolved hyperfine interactions.

The EPR spectra indicate that the ligand field splitting pattern of the t_{2g} orbitals in these complexes is extremely sensitive to

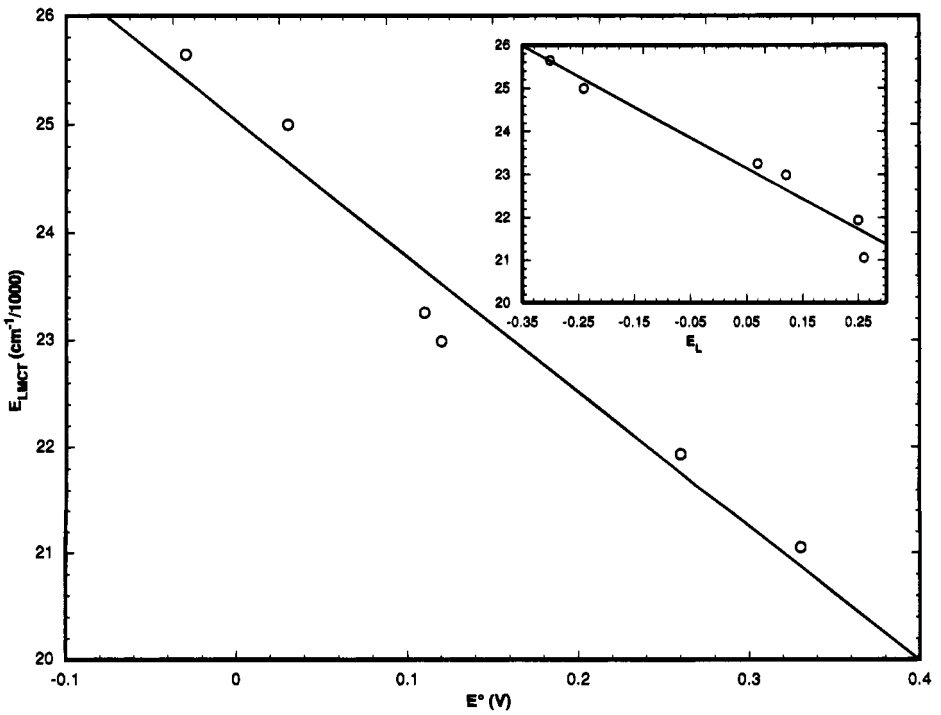

Figure 5. Plot of E_{LMCT} vs $E°$ for $[L(Im)(NH_3)_4Ru^{III}]^{n+}$. $R = 0.96$, the slope = $(-13 \pm 1) \times 10^3$ cm^{-1}/V, and the intercept = $(25 \pm 2) \times 10^3$ cm^{-1}. The inset shows a plot of E_{LMCT} vs E_L for the ligand L in $[L(Im)(NH_3)_4Ru^{III}]^{3+}$. $R = 0.93$, the slope = $(-7 \pm 1) \times 10^3$ cm$^{-1}/E_L$, and the intercept = $(23.5 \pm 0.2) \times 10^3$ cm^{-1}).

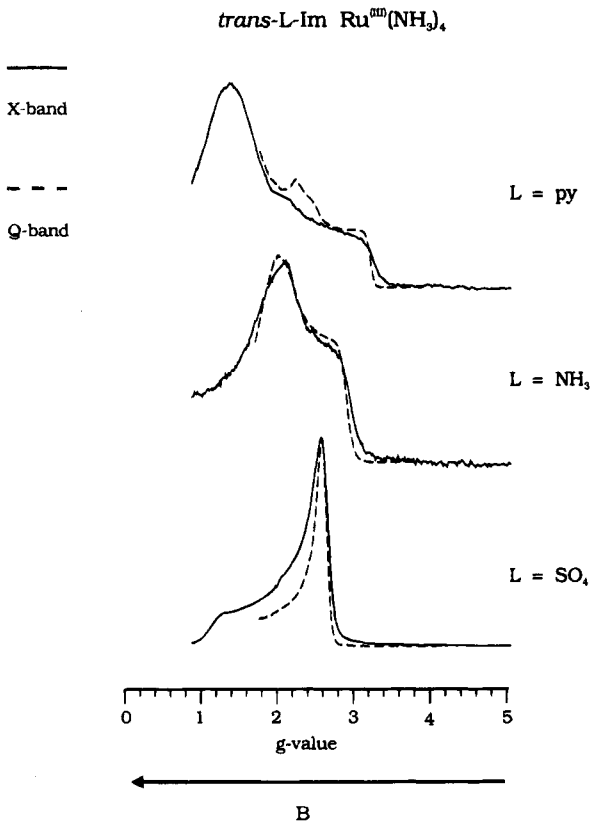

Figure 6. Dispersion mode EPR spectra of *trans*-[L(Im)$(NH_3)_4Ru^{III}$] obtained under rapid passage conditions plotted as a function of **g** value: (a) L = pyridine, (b) L = NH_3, and (c) L = sulfate. Both X-band (—) and Q-band (– –) are shown. Experimental conditions for the X-band spectra are as follows: temperature 2 K; field sweep 0.0500–0.7500 T; modulation amplitude 0.4 mT; time constant 500 ms; sweep time 500 s; 5 transients; microwave power (a) 2 mW, (b) 1 mW, (c) 0.7 mW; microwave frequency (a) 9.63 GHz, (b) 9.65 GHz, (c) 9.60 GHz. Experimental conditions for the Q-band spectra are as follows: temperature 2 K; field sweep 0.6500–1.4500 T; modulation amplitude 0.1 mT; time constant 32 ms; sweep time 480 s; 1 transient; microwave power (a) 0.6 mW, (b) 0.2 mW, (c) 0.1 mW; microwave frequency (a) 34.95 GHz, (b) 35.17 GHz, (c) 35.00 GHz.

the nature of the ligand *trans* to the imidazole. *trans*-$[SO_4(Im)(NH_3)_4Ru^{III}]^+$ shows an axial spectrum, with $g_\perp > g_\parallel$ reflecting a tetragonally elongated complex ($R = 1$), while $[(Im)(NH_3)_5Ru^{III}]^{3+}$ exhibits a Δg_{12} of 0.9, which corresponds to a distinctly rhombic ($R = 0.5$ in Figure 2) EPR pattern. *trans*-$[Py(Im)(NH_3)_4Ru^{III}]^+$ has a large Δg_{12} of 1.8, indicative of a tetragonally compressed complex ($R \approx 0$).

Table 4 summarizes the **g** values for all the compounds studied, together with published values for comparison compounds. The practical cutoff for observing **g** values in frozen solutions was **g** = 0.9 (0.75 T at 9.5 GHz), as **g** strain broadening and base-line difficulties precluded accurate measurements. In the present series of complexes, the smallest **g** value could not be observed (with the exception of the sulfato complex), so that the procedures outlined by Taylor for obtaining ligand field splittings from **g** values could not be used directly. An alternate method was devised in which two crystal field parameters ($(R, \delta e_{13})$ or (Δ, V)) were varied to minimize the function $[(|g_1| - |g_{1calc}|)^2 + (|g_2| - |g_{2calc}|)^2)]$. The g_3 value was restricted to be less than 1.2. The relevant experimental and calculated ligand field parameters (Δ and V) obtained from the fitting of the observed **g** values are given in Table 5.

Since the magnitudes of the ligand field splittings (δe_{12}, δe_{13}) are comparable to λ, the spin–orbit interaction is not quenched but rather extensively mixes the t_{2g} orbitals. In addition, the eigenvalues (ϵ_1, ϵ_2, ϵ_3) show that the ground state lies at least 1.4λ below the first excited state configuration. With 1000 cm^{-1} as an estimate for λ in an Ru^{3+},[22] it is evident there is no significant thermal population ($\Delta e/k_BT \sim 7$) of the excited state doublets at room temperature, so the NMR results can be interpreted by using only the ground state **g** values.[23]

The fraction of tetragonal elongation for $[L(Im)(NH_3)_4Ru^{III}]$ as defined by R correlates well with the π-acidity of L as indicated by $E°$ (see Figure 7), E_L ($R = 0.89$, slope = -0.64 ± 0.09 V, intercept = 0.33 ± 0.05 V), or E_{LMCT} ($R = 0.94$, slope = $(4.7 \pm 0.5) \times 10^3$ cm^{-1}, intercept = $(21.1 \pm 0.3) \times 10^3$ cm^{-1}). The difference between the two largest **g** values, $\Delta g_{12} = g_1 - g_2$, for *trans*-$[L(Im)(NH_3)_4Ru^{III}]$ also correlates with $E°$ (see Figure 7), E_L ($R = 0.87$, slope = 3.1 ± 0.6, intercept = 0.9 ± 0.1), and E_{LMCT} ($R = 0.94$, slope = $(-4.5 \pm 0.5) \times 10^{-4}$ cm, intercept = 11 ± 1).

^{1}H NMR. Because of the paramagnetism of Ru^{III}, the ^{1}H NMR resonances are quite broadened and shifted as shown by the representative spectrum in Figure 9. Assignments of imidazole and pyridine ring proton resonances are based on extensive substitution studies to be published elsewhere.[24]

The isotropic shifts (δ_{iso}) listed in Table 7 represent the shift induced by the metal ion through a combination of contact and pseudocontact (dipolar) interactions. The dipolar component (δ_{dip}) of the isotropic shift was estimated according to the following equation.

$$\delta_{dip} = \frac{\Delta\nu_{dip}}{\nu} = \frac{\mu_0}{4\pi}\frac{\mu_\beta^2 S(S+1)}{9kTr^3}\left\{(3\cos^2\Theta - 1) \times \left(g_z^2 - \frac{g_x^2 + g_y^2}{2}\right) + {}^3/_2 \sin^2\Theta \cos 2\phi\,(g_y^2 - g_x^2)\right\}$$

where μ_0 is the permeability of a vacuum, r is the Ru–H distance, Θ is the angle formed by the Ru–H vector and the $Ru-N_{Im}$ axis, ϕ is the angle from the x-axis of the Ru–H vector projected onto the xy-plane, and μ_β is the Bohr magneton, and the **g** values are given in Table 4 for the compounds studied.[25] The axis system is that shown in Figure 3, with $\cos 2\phi \approx -1$. Values of δ_{con} for the imidazole H5 as estimated from $\delta_{con} = \delta_{iso} - \delta_{dip}$ correlate approximately linearly with $E°$ (see Figure 9) and E_L.

Comparison of δ_{con} values for $[(Im)(NH_3)_5Ru^{III}]$ and the corresponding complex with 2-methylimidazole,[24] which is sterically hindered from rotating, revealed significantly different values for H4 but nearly identical values for H5. This is in harmony with rotation about the z-axis having a negligible effect on H5 ($\Theta = 15°$) but significantly affecting the paramagnetic field for both H4 and H2, which lie at $\Theta = 40°$. Consequently, δ_{dip} and δ_{con} are reported only for H5 in Table 7. Preliminary studies to treat imidazole rotation exactly show that, while the

(20) Krogh-Jespersen, K.; Westbrook, J. D.; Potenza, J. A.; Schugar, H. J. *J. Am. Chem. Soc.* **1987**, *109*, 7025–7031.
(21) Lever, A. B. P. *Inorg. Chem.* **1990**, *29*, 1271–1285.
(22) Bunker, B. C.; Drago, R. S.; Hendrickson, D. N.; Richman, R. M.; Kessell, S. L. *J. Am. Chem. Soc.* **1978**, *100*, 3805–3814.
(23) Kurland, R. J.; McGarvey, B. R. *J. Magn. Reson.* **1970**, *2*, 286–301.
(24) Rodriguez-Bailey, V. Ph.D. Thesis, Boston College, 1992.
(25) Bertini, I.; Luchinat, C. *NMR of Paramagnetic Molecules in Biological Systems*; Benjamin Cummings: San Francisco, CA, 1986; pp 36–38.
(26) Kastner, M. E.; Coffey, K. F.; Clarke, M. J.; Edmonds, S. E.; Eriks, K. *J. Am. Chem. Soc.* **1981**, *103*, 5747–5752.
(27) John, E.; Schugar, H. J.; Potenza, J. A. *Acta Crystallogr., Sect. C: Cryst. Struct. Commun.* **1992**, *48*, 1574.
(28) Stynes, H. C.; Ibers, J. A. *Inorg. Chem.* **1971**, *10*, 2304.
(29) Wishart, J. F.; Bino, A.; Taube, H. *Inorg. Chem.* **1986**, *25*, 3318–3321.
(30) Richardson, D. E.; Walker, D. D.; Sutton, J. E.; Hodgson, K. O.; Taube, H. *Inorg. Chem.* **1979**, *18*, 2216.

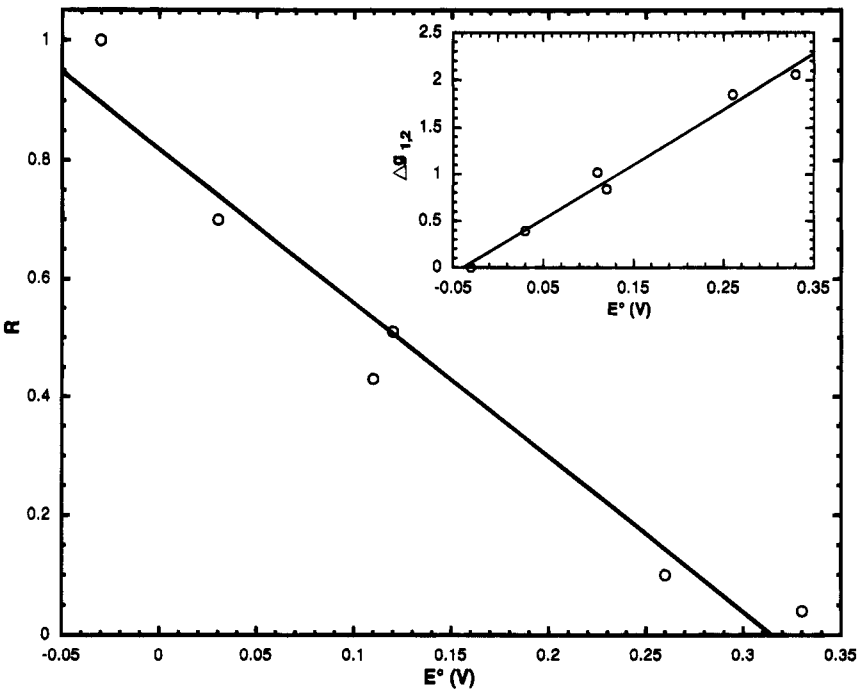

Figure 7. Plot of the degree of fractional tetragonal elongation (R) vs $E°$ in *trans*-[L(Im)$(NH_3)_4Ru^{III}$]. $R = 0.94$, the slope $= -0.36 \pm 0.04$ V, and the intercept $= 0.30 \pm 0.02$ V. the inset shows a plot of Δg_{12} vs $E°$. $R = 0.99$, the slope $= 5.9 \pm 0.3$ V^{-1}, and the intercept $= 0.21 \pm 0.06$.

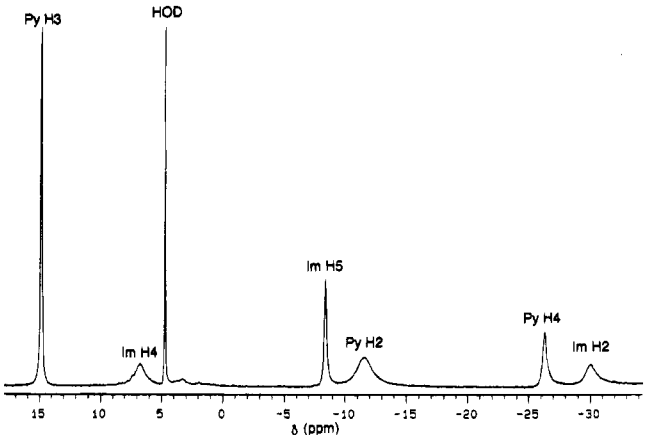

Figure 8. ^1H NMR spectra of *trans*-$[Py(Im)(NH_3)_4Ru^{III}]^{n+}$ in D_2O with pD ~ 5 at 23 °C.

Table 6. Ground State (ϵ_1) Coefficients of the Hole States for $[(L)(L')(NH_3)_4Ru^{III}]$ and Percentage Hole Character in the d_{xz} Orbital

complex[a]	T_{xz}	T_{yz}	T_{xy}	% d_{xz} (T_{xz}^2)
trans-Im$-SO_4^{2-}$	0.932	0.257	0.257	87
trans-Im$-Cl^-$	0.931	0.288	0.222	87
trans-Im$-$Im	0.798	0.487	0.355	64
trans-Im$-NH_3$	0.757	0.521	0.394	57
trans-Im$-$Py	0.693	0.631	0.349	48
trans-Im$-$Isn	0.679	0.652	0.337	46
trans-NH_3-Py[a]	0.693	0.631	0.349	
trans-Cl$-NH_3$[a]	0.689	0.611	0.389	

[a] Symmetry labels not assigned.

predicted effects of such rotation on the ground electronic states of these compounds are extremely complicated, the present treatment yields good estimates for H.

Discussion

Structure. The $Ru-NH_3$ distances are within the average $Ru^{III}-NH_3$ distance of 2.105(18) Å derived from 10 other crystal structures.[2,20,26-30] The average $Ru-N_{Im}$ distance (2.049(4) Å) is significantly shorter than those found in pentaammineruthenium(III) complexes of hypoxanthine (2.087(9) Å) and 7-methylhypoxanthine (2.094(6) Å),[26] in which the coordinated nitrogen is substantially less basic than in imidazole, but only possibly significantly shorter than that in the analogous 7-methylguanine complex (2.073(5) Å), in which the guanine amine increases the donor ability of the ligand.[31] The distances reported here are essentially identical to that in *trans*-[(Im)(Isn)$(NH_3)_4Ru^{III}]^{3+}$ (2.049(7) Å)[2] and not significantly longer than that in $[(His)(NH_3)_5Ru^{III}]^{3+}$ (2.020(8) Å). Relative to bonds involving other sp^2 nitrogens, the $Ru-N_{Im}$ distances reported here are not significantly shorter than an average of four $Ru-N_{py}$ and $Ru-N_{pz}$ distances (2.089(11) Å).[2,29,30,32] Consequently, while Ru−N distances generally follow in the sequence $N_{amine} > N_{Py} > N_{Im}$, the differences are frequently not statistically significant, so variations in bonding between these three types of ligands are not structurally dominant.

The eclipsed conformation of the two imidazoles in the *trans* complex arises partly from steric effects, which are minimized by having the two imidazoles in the same plane with the ammonias bent away from this plane. MM2 calculations indicate that this arrangement is 1.4 kJ mol^{-1} lower in energy than the staggered conformation. The eclipsed conformation should also be favored as it leads to a nondegenerate orbital ground state (d_{xz}^1, d_{yz}^2, $d_{x^2-y^2}^2$), since both imidazoles undergo π-interactions with a single orbital (d_{xz}), as opposed to the staggered conformation, which leads to a doubly degenerate orbital ground state ((d_{xz}, $d_{yz})^3$, $d_{x^2-y^2}^2$). Assuming noninteracting imidazoles, spin−orbit effects alone predict the eclipsed conformation to be about 0.8 kJ mol^{-1} (70 cm^{-1}) lower in energy than the staggered conformation.

Similar arguments have been made concerning the effect of staggered vs eclipsed configurations on the reduction potential of cytochrome *b*.[33] Moreover, differences in $\pi-d_\pi$ orbital mixing between the two configurations would yield markedly

(31) Rodriguez-Bailey, V. M.; LaChance-Galang, K.; Clarke, M. J. Unpublished results, 1994.
(32) Gress, M. E.; Creutz, C.; Quicksall, C. O. *Inorg. Chem.* **1981**, *20*, 1522.
(33) Walker, F. A.; Huynh, B. H.; Scheidt, W. R.; Osvath, S. R. *J. Am. Chem. Soc.* **1986**, *108*, 5288−5297.

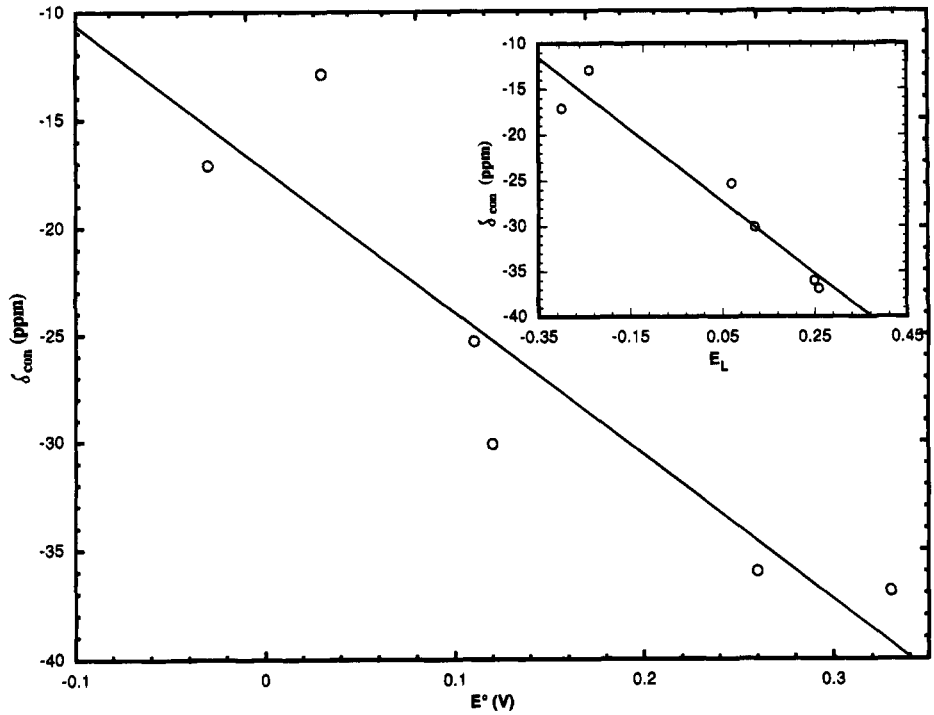

Figure 9. Plot of δ_{con} (H5) vs $E°$ for *trans*-[L(Im)$(NH_3)_4Ru^{III}]^{n+}$. $R = 0.86$, the slope $= -67 \pm 13$, and the intercept $= -17 \pm 2$. The inset shows a plot of δ_{con} (H5) vs E_L. $R = 0.94$, the slope $= -39 \pm 5$, and the intercept $= -25 \pm 1$).

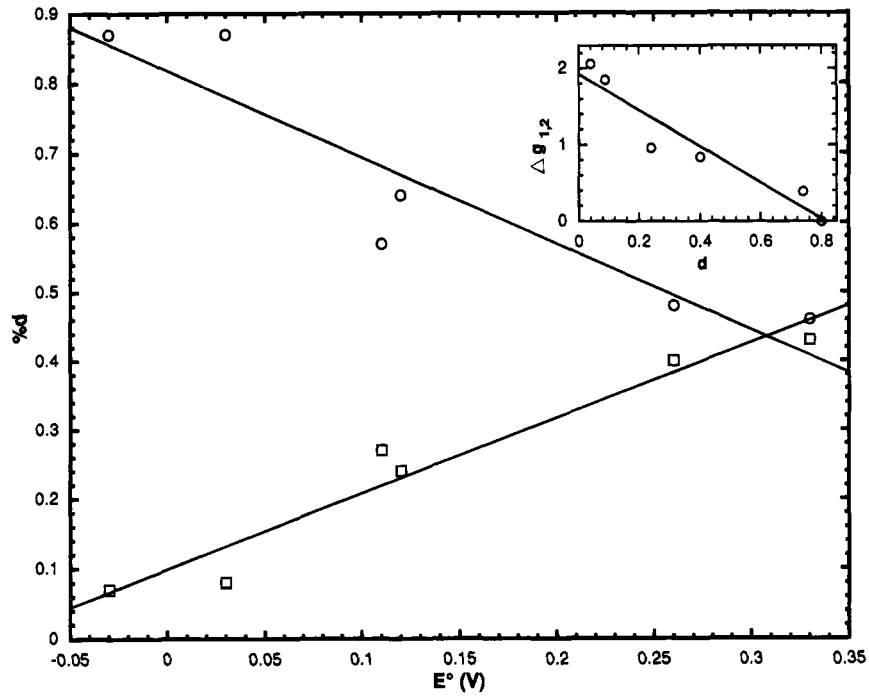

Figure 10. Plot of fraction of d orbital character (O, d_{xz}; □, d_{yz}) in the ground state vs $E°$. For fraction of d_{xz} vs $E°$, the slope $= -1.24 \pm 0.24$, the intercept $= 0.82 \pm 0.04$, and $R = 0.86$. For fraction of d_{yz} vs $E°$, the slope $= 1.09 \pm 0.13$, the intercept $= 0.10 \pm 0.02$, and $R = 0.94$. The fraction of d_{xy} is relatively constant at 0.11 ± 0.04. The inset shows a plot of Δg_{12} vs Δd (fraction d_{xz} − fraction d_{yz} in the ground state) with the slope $= -2.3 \pm 0.3$, the intercept $= 2.0 \pm 0.2$, and $R = 0.92$.

different g values.[33,34] The staggered conformer is tetragonally compressed ($R = 0$) and should be characterized by a large Δg_{12}, similar to that seen for *trans*-[(Im)(Isn)$(NH_3)_4Ru^{III}]^{3+}$. The g values observed in the solid samples at 77 K are essentially the same as the g values in the frozen solution for all complexes, indicating that the solid state structure is maintained in the frozen solution.

UV−Vis Spectra and Electrochemistry. The reduction potentials exhibit the expected correlation with the π-donor/acceptor ability of the ligand to transfer electron density to Ru^{III} or delocalize electron density from Ru^{II}. The correlations between E_{LMCT} and $E°$ and the Lever parameter for the *trans* ligand indicate a substantial ability of the *trans* ligand to affect the energy of the LMCT acceptor orbital, which is substantially d_{xz} in character.[2] It is likely that this occurs by increased mixing of the ligand π and metal d_{xz} orbitals with increasing π-acceptor ability of the ligand *trans* to the π-donor imidazole. Since this involves increasing incorporation of a lower-energy ligand π^* orbital into the HOMO with increasing π-acceptor character of the *trans* ligand, E_{LMCT} decreases with increasing $E°$, yielding the negative slope shown in Figure 5. Not surprisingly, E_{LMCT}

(34) Telser, J.; Drago, R. S. Personal communication, 1995.

Table 7. ^{1}H NMR Chemical Shifts for Heterocyclic Ligands in $[(L)(L')(NH_3)_4Ru^{III}]$[a]

L–L′	proton	δ (ppm)	δ_{dia}[e] (ppm)	δ_{iso} (ppm)	δ_{dip} (ppm)	δ_{con} (ppm)
trans-Im–SO_4^{2-}	H2	−49.1	8.05	−57.2		
	H4	5.4	7.46	-2.1		
	H5	−3	7.07	−10.1	7.0	−17.1
trans-Im–SO_4^{2-}[b]	H2	−58.6	7.44	−66.0		
	H4	12.2	7.24	5.0		
	H5	−45	6.91	−51.9		
trans-Im–Cl^-	H2	−34.41	8.05	−42.5		
	H4	9.79	7.46	2.3		
	H5	4.54	7.07	−2.5	10.3	−12.9
trans-Im–Cl[b]	H2	−44.4	7.44	−51.8		
	H4	1.3	7.24	−5.9		
	H5	−24.7	6.91	−31.6		
trans-Im–Im	H2	−37.79	8.05	−45.8		
	H4	9.31	7.46	1.9		
	H5	−7.35	7.07	−14.4	15.7	−30.1
trans-Im–Im[c]	H2	−46.1	7.44	−53.5		
	H4	12.4	7.24	5.2		
	H5	−36.3	6.91	−43.2		
trans-Im–NH_3	H2	−27.02	8.05	−35.1		
	H4	3.24	7.46	−4.2		
	H5	−3.01	7.07	−10.1	15.2	−25.3
trans-Im–NH_3[b]	H2	−29.21	7.44	−36.7		
	H4	3.14	7.24	−4.1		
	H5	−8.48	6.91	−15.4		
trans-Im–Py	H2	−30.02	8.05	−38.1		
	H4	6.76	7.46	−0.7		
	H5	−8.40	7.07	−15.5	20.5	−36.0
	Py–H2	−11.66	8.41	−20.1		
	Py–H3	14.88	7.35	7.5		
	Py–H4	−26.29	7.76	−34.1		
trans-Im–Isn	H2	−28.53	8.05	−36.6		
	H4	5[c]	7.46			
	H5	−8.73	7.07	−15.8	21.1	−36.9
	Isn–H2	−11.10	7.55	−18.7		
	Isn–H3	13.90	8.5	5.4		

[a] The numbering system is

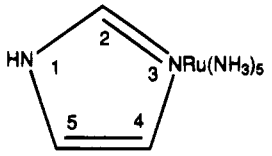

[b] Imidazole ionized. [c] Both imidazoles ionized. [d] Peak obscured by HOD resonance. [e] For δ_{dia}'s of imidazole and imidazolate, the heterocyclic proton resonances in $[Im(NH_3)_5Co]^{3+}$ and $[Im(NH_3)_5Co]^{2+}$ are used.[43] For pyridine, there were free ligand resonances.

and $E°$ also correlate with the tetragonal distortion parameter, Δ, and R since all depend on the net donor/acceptor ability of L. Correlations between Δg_{12} and E_{LMCT} and $E°$ are discussed below.

EPR Spectra: g Tensor Directions. EPR spectra obtained in frozen solution yield only the ligand field energy splitting patterns, and an interpretation in terms of proper EPR axes refers to an undetermined magnetic axis system. While single-crystal EPR data are needed to unequivocally map the **g** tensor to the crystallographic axes and thereby onto the coordination axes, the compounds studied here are sufficiently similar to those for which single-crystal data are available so as to provide a guide to preliminary assignments.[20,35–37]

Single-crystal polarized LMCT spectra and detailed molecular orbital calculations for $[(His)(NH_3)_5Ru^{III}]Cl_3$ led to the conclusion that the d_{xz} orbital contains the unpaired spin so that d_π–p_π interactions are maximized.[20] This is in harmony with the above inference that π-donation by the imidazole ring raises the energy of the d_{xz} orbital above that of both the d_{xy} and d_{yz} orbitals. The EPR-derived parameters for $[Im(NH_3)_5Ru^{III}]$ show a distinctly rhombic complex that is energetically tetragonally compressed ($R < 0.5$) with nearly equal energy spacings $\delta e_{12} \approx \delta e_{23} \approx 0.5\ \lambda$ (ca. 500 cm^{-1}). If the highest-lying d orbital is taken to be d_{xz}, then g_3 lies along the x axis, which is normal to the plane of the imidazole. The ligand field energy order of the $d_{x^2-y^2}$ and d_{yz} orbitals then determines the orientations of g_1 and g_2. Since imidazole hydrogen atoms impinge on the d_{yz} lobes, the more likely order is for the d_{yz} orbital to lie above the $d_{x^2-y^2}$. Consequently, g_1 is placed along the z-axis and g_2 along the y-axis. The small ligand field energy splittings relative to λ cause the orbitals to be extensively mixed so that the ground state has only 54% T_{xz} character, in contrast to the essentially 100% character previously assigned.[20]

By analogy, and consistent with the IEHT calculations, the d orbital energies in *trans*-$[(Im)_2(NH_3)_4Ru^{III}]^{3+}$ can also be ordered as $d_{xz} > d_{yz} > d_{x^2-y^2}$. This orbital ordering produces the same **g** value assignments as in $[(Im)(NH_3)_5Ru^{III}]^{3+}$: $g_1 = g_z$, $g_2 = g_y$, and $g_3 = g_x$. The addition of a second imidazole further destabilizes d_{xz} with respect to d_{yz} and $d_{x^2-y^2}$, thereby more effectively quenching the mixing of configurations to give an electronic ground state with a higher percentage of T_{xz} (cf. Table 6 and Figure 10).

The two complexes with anionic sixth ligands display tetragonally elongated systems, with relatively large values of $|\delta e_{13}/\lambda|$ (see Table 5). A single-crystal study of $[Cl(NH_3)_5Ru]Cl_2$ (see Tables 5 and 6) showed that the chloride acts as a π-donor by raising the energies of both the d_{xz} and d_{yz} orbitals with respect to the d_{xy} orbital.[35–37] The addition of a second π-donor (Im, Cl^-, SO_4^{2-}) should further destabilize the d_{xz} orbital so that it is expected to be the HOMO. The large energy splittings between d_{xz} and the d_2 and d_3 levels means that the spin–orbit mixing is less and the ground state configuration is closer to a pure T_{xz} (cf. Table 6). For the sulfato complex, d_{yz} and $d_{x^2-y^2}$ are degenerate, so that $g_1 = g_2 = g_z, g_y$ and g_3 is assigned to g_x. The more likely ordering for *trans*-Im–Cl is $d_{yz} > d_{x^2-y^2}$ so that $g_1 = g_z$, $g_2 = g_y$, and $g_3 = g_x$.

The spectra for complexes with π-acceptor ligands (L = Py, Isn) are approximately the mirror image of the spectra for L = π-donor complexes (Figure 7). Continuing the assumption that π-interactions dominate the splittings, we find that the spectrum of $[Py(NH_3)_5Ru^{III}]$ corresponds to a tetragonally compressed ($\delta e_{12} \ll \delta e_{13}$) electronic structure with some degree of rhombicity. The *trans*-Im–Py and *trans*-Im–Isn complexes are effectively tetragonally distorted, leading to a doubly degenerate orbital ground state, in which the two HOMO d orbitals are *extensively* mixed by the spin–orbit interaction, so that the ground state is less than 50% of any individual T orbital.

The co-planarity of the two heterocyclic ligands in *trans*-Im–Isn suggested that the π-interaction between these ligands is maximized, and the similarity of the LMCT band in the *trans*-

(35) Kaplan, D.; Narvon, G. *J. Phys. Chem.* **1974**, *78*, 700–703.
(36) Carlin, R. L.; Burriel, R.; Seddon, K. R.; Crisp, R. I. *Inorg. Chem.* **1982**, *21*, 4337–4338.
(37) Carlin, R. L. *Magnetochemistry*; Springer-Verlag: New York, 1986.
(38) Ibers, J. A.; Hamilton, W. C. *Acta Crystallogr.* **1964**, *17*, 781–782.
(39) Gilmore, C. J. *J. Appl. Crystallogr.* **1984**, *17*, 42–46.
(40) Beurskens, P. T. DIRDIF. Techical Report No. 1984/1; Crystallographic Laboratory: Toernooiveld, Nijmegen, The Netherlands, 1984.
(41) Ford, P.; Rudd, D. F. P.; Gaunder, R.; Taube, H. *J. Am. Chem. Soc.* **1968**, *90*, 1187–1194.
(42) Sakaki, S.; Yanase, Y.; Hagiwara, N.; Takeshita, T.; Naganuma, H.; Ohyoshi, A.; Ohkubo, K. *J. Phys. Chem.* **1982**, *86*, 1038–1043.
(43) Rowan, N. S.; Storm, C. B.; Rowan, R. *J. Inorg. Biochem.* **1981**, *14*, 59–65.
(44) Hori, H. *Biochim. Biophys. Acta* **1971**, *251*, 227–235.
(45) Hush, N. S.; Edgar, A.; Beattie, I. R. *Chem. Phys. Lett.* **1980**, *69*, 128–133.
(46) Wang, D. M.; de Boer, E. *J. Chem. Phys.* **1990**, *92*, 4698.
(47) Sundberg, R. J.; Gupta, G. *Bioinorg. Chem.* **1973**, *3*, 39–48.

Im−Isn and *trans*-Im−NH_3 complexes was taken to imply that the unpaired spin was in an orbital of similar symmetry in both complexes.[2] However, the coefficients listed in Table 6 indicate that two d orbitals contribute nearly equally in the *trans*-Im−Py and *trans*-Im−Isn complexes, so that the unpaired spin cannot readily be assigned to a single d orbital. Using the same reasoning as in the four previous examples, we find that the two highest lying orbitals are expected to be d_{xz} and d_{yz}, causing g_1 to be assigned to the z-axis as in other systems. Apparently, the π-acceptor pyridine ligand lowers the energy of the d_{xz} orbital by about the same amount that the π-donor imidazole raises it. Consequently, it is difficult to assign the highest energy orbital with any confidence. However, the large differences between $(g_1)^2$ and $(g_{23})^2$ for these systems makes the assignments of the axes for the smaller g values less important for the NMR shift calculations.

The EPR spectra of $[Py(NH_3)_5Ru^{III}]$ exhibit much broader lines than the other complexes so that the **g** values are difficult to determine even at 35 GHz. In contrast to $[Im(NH_3)_5Ru^{III}]$, the X-band EPR spectra suggest $g_3 > 1$, as the pattern returns to base line by 0.7 T, but there is no well-defined inflection in the curve that can be assigned a **g** value. Consequently, the values listed in Table 4 for this complex are only approximate.

Tables 5 and 6 show EPR spectroscopy to be an effective tool for determining the nature of the ground state in complexes of the type *trans*-$[L(Im)(NH_3)_5Ru^{III}]$. The spin Hamiltonian parameters derived for these complexes shows that the ligand field splittings in the t_{2g} manifold are approximately the same size as the spin−orbit coupling parameter ($\lambda \approx 1000$ cm^{-1} = 11.97 kJ), so that mixing of the spatial orbitals by spin−orbit interaction should not be ignored. The ground state is quite sensitive to the nature of the ligand *trans* to the imidazole, whose π-donor properties dispose the d_{xz} orbital to make a significant contribution to the electronic ground state. Placing a π-accepting ligand (Py or Isn) *trans* to the imidazole leads to a strongly mixed ground state, with no single d orbital contributing more than half to the character of the ground state, so that unambiguous assignments cannot be made in such cases. Finally, even though the ligand field interaction does not effectively quench the spin−orbit interaction, there are no magnetic excited states with significant populations at room temperature. Consequently, the paramagnetic effects seen in the ^{1}H NMR results are the result of ground state magnetic effects.

^{1}H NMR. The strongly shifted and broadened heterocyclic proton resonances are typical for Ru^{III} complexes.[24] Since δ_{con} for the imidazole H5 decreases dramatically with $E°$ (Figure 8) and E_L (i.e. with π-acceptor ability of the *trans* ligand), hyperfine coupling through C5 is directly affected by the π-donor/acceptor ability of the *trans* ligand in such a way as to transfer ↑-spin onto the π-MO of the imidazole. This is in keeping with a concept of π-electron density from the imidazole being attracted onto Ru^{III} by means of a *trans* π-acceptor ligand (or kept from the metal ion by a *trans* π-donor) so that the d_{xz} orbital participates more (or less) in a MO extending to C5. This suggests that electronic coupling ($\mathbf{H}_{AB}$) through this site increases with $E°$, so that electron transfer to Ru^{III} increases through both the $\Delta\mathbf{G}$ and $\mathbf{H}_{AB}$ terms. By the same token, electron transfer from Ru^{II} interacting with a π^*−imidazole orbital might be expected to decrease, also on both accounts.

Conclusion. EPR and NMR studies provide strong indications that varying the ligands *trans* to the histidylimidazole to modulate $E°$ also modulates the coupling between the ruthenium d_π orbitals and those of the C5 on the imidazole ring. Consequently, a ligand-induced change in the driving force ($-\Delta\mathbf{G}°$) for electron transfer in the Marcus equation (eq 1) also alters the coupling or overlap term $\mathbf{H}_{AB}$. The matrix element $\mathbf{H}_{AB}$ is roughly proportional to the hole coefficient of the d_{xz} orbital in the ground state (T_{xz}), and so k_{ET} is proportional to T_{xz}^2, the percentage of hole character in the d_{xz} orbital, which can be determined directly from EPR.

For the compounds in this study, Figure 10 indicates about 12% change in hole character of d_{xz} for every 100 mV change in $E°$ and Table 6 shows that hole character varies over almost a factor of 2 from 87% for the anionic, π-donor ligands to 46% for the π-acceptor, isonicotinamide ligand. The range is smaller for the subset of ligands (Im, 64% through Isn, 46%) that is used commonly in studies of long-range electron transfer through proteins. This calculation yields a lower limit because the analysis assumes that the highest lying t_{2g} orbital (d_1) is d_{xz} for all the complexes studied. The upper limit can be calculated by assuming that there is an actual flip in the hole orbital with d_{xz} orbital being d_1 in *trans*-$[(Im)_2(NH_3)_4Ru]^{3+}$ and d_3 in *trans*-$[(Im)(Isn)(NH_3)_4Ru]^{3+}$. If this were so, the difference in $\mathbf{H}_{AB}^2$ between the two molecules would be a factor of 6 (0.64/0.11).

Clearly, it is fortunate for the use of these compounds in electron transfer studies that the extensive spin−orbit mixing of the d orbitals in these systems yields ground states with relatively large percentages of all the d_π orbitals (10−90%), so that a change in $\mathbf{H}_{AB}^2$ by a factor of 6−8 is the largest expected for varying a single *trans* ligand. The range of $\mathbf{H}_{AB}^2$ might be expected to increase as more π-donor or π-acceptor ligands are added.

Acknowledgment. Work at Boston College was funded by NIH Grant GM26390. Work at Northwestern University was funded by NIH Grant HL13531. P.E.D. and B.M.H. acknowledge the expert technical assistance of Mr. Clark E. Davoust.

Supplementary Material Available: Explanation of the **g** tensor rotation; tables of crystallographic data, atomic positions and isotropic parameters, bond angles involving the non-hydrogen atoms, bond distances involving hydrogen and non-hydrogen atoms, least-squares planes, UV−vis spectra, and pK_a's; and a figure of the spectra of *cis*- and *trans*-$[(Im)(NH_3)_4Ru]^{3+}$ in water (18 pages). This material is contained in many libraries on microfiche, immediately follows this article in the microfilm version of the journal, can be ordered from the ACS, and can be downloaded from the Internet; see any current masthead page for ordering information and Internet access instructions.

JA942541S